Available online at www.sciencedirect.com
SCIENCE DIRECT®
Journal of Crystal Growth 266 (2004) 246–256
JOURNAL OF CRYSTAL GROWTH
www.elsevier.com/locate/jcrysgro

Experimental and numerical analysis of coupled interfacial kinetics and heat transport during the axial heat flux close to the phase interface growth of BGO single crystals

S.V. Bykova[a], V.D. Golyshev[a], M.A. Gonik[a,*], V.B. Tsvetovsky[a], V.I. Deshko[b], A.Ya. Karvatskii[b], A.V. Lenkin[b], S. Brandon[c], O. Weinstein[c], A. Virozub[c], J.J. Derby[d], A. Yeckel[d], P. Sonda[d]

[a] *Center for Thermophysical Researches "Thermo", Alexandrov, Russia*
[b] *Kiev Polytechnic Institute, Kiev, Ukraine*
[c] *Department of Chemical Engineering, Technion, Haifa, Israel*
[d] *Department of Chemical Engineering and Materials Science, University of Minnesota, Minneapolis, MN, USA*

Abstract

Combined experimental and numerical tools are used to analyze the effect of convective and radiative heat transport, faceting phenomena, and the optical thickness of the $Bi_4Ge_3O_{12}$ (BGO) crystal on the measurement and calculation of melt/crystal interface kinetics during the axial heat flux close to the phase interface growth of BGO single crystals. Results show that, in the general case, accurate determination of growth kinetic relations requires the application of models which account for all of the above phenomena (radiative and convective heat transport, faceting phenomena, etc.). Failure to take these into account may result not only in quantitative errors, but also even in qualitatively wrong determination of interfacial kinetic mechanisms.

PACS: 81.10.Aj; 81.10.Fq; 68.08.P; 68.08.De

Keywords: A1. Interfaces; A2. Growth from melt; B1. Bismuth germanate

1. Introduction

The recent development of a method for the determination of temperature at the melt/crystal interface, by recording of thermal radiation from the interface with a pyrometer [1], has made possible in situ measurements of facet undercooling (ΔT) during the melt growth of $Bi_4Ge_3O_{12}$ (BGO) crystals [2]. However, the experimentally measured values of $\Delta T = 3-5$ K, averaged over the pyrometer measuring spot, require adjustments. In Ref. [3] the undercooling was recalculated taking into account the actual interface morphology resulting in a considerable, $\Delta T = 12-17$ K, undercooling value for the (2 1 1) facet. Estimates have also shown a 4–5 K variation of undercooling along the facet [4]. Finally, recent work [5] shows that the technique of undercooling measurement under discussion

*Corresponding author. Fax: +7-095-584-5816.
E-mail address: thermo.ltd@relcom.ru (M.A. Gonik).

0022-0248/$ - see front matter © 2004 Elsevier B.V. All rights reserved.
doi:10.1016/j.jcrysgro.2004.02.052

requires a correction to the measured values of ΔT in cases when the crystal's optical absorption coefficient exceeds some limiting value.

The recording of the time-dependent undercooling $\Delta T(t)$, together with the simultaneous measurement of the temperature distribution along boundaries of the melt–crystal system [1,2], made it possible to calculate [6,7] the dependence of growth rate on time $V(t)$ and build a functional dependence of growth rate on undercooling $V = f(\Delta T)$. Surprisingly, this dependence appeared to exhibit sublinear behavior [3,8], which is in contrast to the theoretically predicted superlinear dependence of V versus ΔT [9]. To explain this, it has been suggested [10] that the interfacial kinetics growth mechanism may change with changing BGO growth rate. However, the unexpected $V(\Delta T)$ dependence obtained in Refs. [3,8] can also be explained by an inaccuracy in determining the time dependence of growth rate, caused by employment of a rather crude one-dimensional model of heat transfer. The technique for determination of growth-rate dependence on undercooling for this in situ method therefore requires further improvement. This is of utmost importance when considering the advantages of applying this novel approach to obtain data on interfacial kinetics for a family of technologically important single crystals.

In this paper we focus on the experimental and numerical analysis of the influence of sample optical absorption, various mechanisms of heat transport, as well as faceting phenomena on the dynamics of undercooling and growth rate during in situ measurement of undercooling with the method under consideration.

2. Experimental and numerical procedures

2.1. Experimental description

To determine the $V(\Delta T)$ dependence, both numerical methods and experimental equipment were developed. The time variation of ΔT is determined by measuring the interface brightness temperature, T_b, through the growing crystal using an optical pyrometer (Fig. 1). Theoretical principles of the method and technique for measurement of undercooling are described in detail in Refs. [2,7,8]. Implementation of the method is possible due to a favorable combination of high-temperature optical properties of BGO melt and crystal [11]. In the wavelength range of 0.35–4 μm a BGO crystal has a very small absorption coefficient value, $\alpha_1 = 0.002-0.04\,\mathrm{cm}^{-1}$, depending on its quality [12]. If both absorption and re-radiation in the crystal are neglected, one may consider the radiation from the melt to propagate through the crystal without any change. Due to the large optical absorption of the melt, α_2, the thermal radiation of the melt originates from a thin melt layer adjoining the crystal. Therefore, the level of this radiation is essentially determined by the temperature of the interface. For this case, the changing of brightness temperature with variation of growth rate is caused only by changes in interface temperature, i.e., by undercooling of the interface of the growing crystal. The value of ΔT was found as $\Delta T = T_{bm} - T_{bi}$, where T_{bm} is the brightness temperature measured by pyrometer without crystal growth, T_{bi} is the brightness temperature measured by pyrometer during crystal growth.

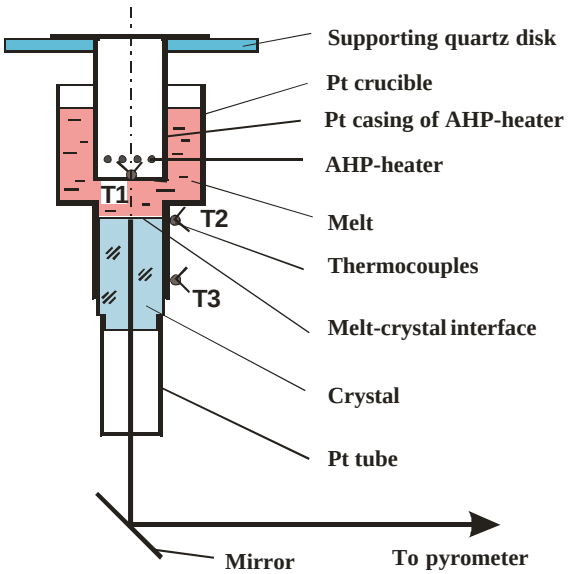

Fig. 1. Schematic of AHP crystallizer for measurements of interfacial undercooling.

The axial heat flux close to the phase interface growth method (AHP method) [13] was employed as a tool for in situ investigations of undercooling. A schematic of the experimental setup is shown in Fig. 1. A 25 mm diameter BGO single crystal with polished ends was used as a seed. The crystal was placed in the lower part of the platinum crucible, with the bottom end of the crystal extending through the bottom of the crucible and the top end initially in contact with the bottom of the platinum AHP-heater casing. The temperature at the interface was measured through the bottom end of the crystal. The thickness of the crucible wall and AHP-heater casing were 0.2 mm. The standard disappearing-filament optical pyrometer LOP-72 was used to measure T_b, where the diameter of the measuring spot of the pyrometer was 8 mm, and its wavelength was 0.65 μm.

Experimental investigations of undercooling were conducted using two crystallization methods: the AHP method (method A) and the melt cooling method (method B). The BGO single crystals used in these experiments were annealed before the in situ experiments were conducted. They were of white color and stoichiometric composition. For both of the methods, the goal of the in situ undercooling experiments was the determination of the time dependence of the undercooling $\Delta T(t)$.

In method A, melt was obtained in the upper part of the crucible (50 mm in diameter) by placing pieces of BGO single crystals into the crucible around the AHP-heater casing. Growth of a BGO crystal in the [1 1 0] direction was realized by translating the crucible and crystal downwards relative to the stationary AHP-heater [8]. During this experiment approximately 10 mm of new crystal was grown in 130 min. Additional details of the experimental procedure are given in Ref. [4]. The calculation domain for this case is shown in Fig. 2a.

In method B, no additional charge was put into the crucible and all parts of the system were held stationary. The top end of the crystal was initially melted using the AHP-heater to create a thin layer of melt approximately 3 mm in depth. The melt remained connected to the bottom of the AHP-heater casing through surface tension forces, preventing it from flowing out from under the AHP-heater. However, a thin air bubble, approximately 0.5 mm in thickness, was formed under the center part of the AHP-heater [3]. The melt was subsequently cooled at a specified rate by reducing power to the AHP-heater, causing growth of a (2 1 1) facet. During this experiment approximately 3 mm of crystal was grown over times ranging from 20 to 60 min, depending on the cooling rate. Additional details of the experimental procedure are given in Ref. [3]. The calculation domain for this case is shown in Fig. 2b.

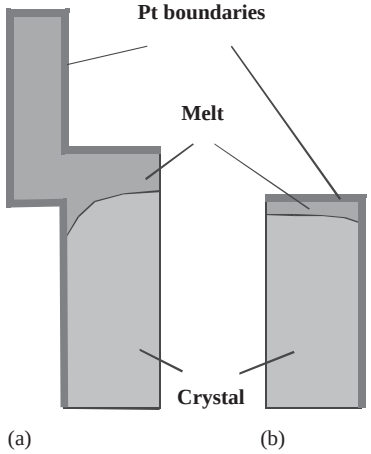

Fig. 2. Geometry of calculation domain in crystal growth via crucible pulling with a crystal downwards (a) and via the cooling method of the AHP heater (b).

Although single crystal BGO is highly transparent to thermal radiation, the absorption and reradiation in the crystal affects pyrometer readings, as was shown in Ref. [5]. The effect of the optical thickness of the sample ($\tau = \alpha_1 H$, where H is the crystal height and α_1 is the absorption coefficient) on pyrometer-based measurements was therefore investigated; the dependence of brightness temperature on crystal height and crystal temperature distribution was studied by numerical and experimental methods. The influence of crystal temperature distribution was studied using a solid sample without melting, while the influence of crystal height was studied by comparing the pyrometer readings during melting and crystallization processes. A special-purpose pyrometer [14], operating at wavelengths of $\lambda_1 = 0.795$ and $\lambda_2 = 0.995$ μm, with a 0.1 K resolution in the

temperature range of 1100–1400 K and a measuring spot size of 1.2 mm, was utilized for these studies. During these measurements, the pyrometer was mounted directly along the axis of the sample without use of the mirror shown in Fig. 1.

2.2. Description of the numerical models

Four different Stefan-type models were employed for the analysis of various phenomena related to the dynamics of crystal growth during in situ undercooling measurements. Model I is a 2D model that focuses on melt convection, model II is a 2D model that focuses on internal thermal radiation, model III is a 2D model that focuses on anisotropic interface kinetics, and model IV is a 3D model that focuses on facet formation. Additional details of each model are provided below. The models were employed for multiple reasons: to characterize the effect of thermal convection (models I and III) and crystal optical properties (model II) on the experiments, to determine the $V(\Delta T)$ dependence using $\Delta T(t)$ experimental data (models I and II), and to determine the influence of kinetic mechanism on $V(t)$ and $\Delta T(t)$ (models III and IV). The thermal boundary condition for the crucible wall was obtained by a least-squares fit of the experimental data to the function $T_{\text{wall}} = b_0 + b_1 z + b_2 t + b_3 z t + b_4 z^2 + b_5 t^2$. The experimental data, described in Ref. [4] for method A and in Ref. [3] for method B, were used to simulate in situ undercooling experiments.

In model I, the temperature at the melt/crystal interface was taken to be equal to the BGO melting point less than the interface undercooling: $T_{\text{i}} = T_{\text{m}} - \Delta T$. Faceting of the interface was not considered and undercooling was assumed to be independent of position on the interface. The undercooling ΔT varied with time, with the $\Delta T(t)$ dependence obtained by fitting experimental data to a quadratic function. Crystal growth was modeled using equations similar to those found in Yeckel et al. [15], which include thermal conduction and buoyancy-driven melt convection. For the geometry in Fig. 2b, the gas bubble described above was included in the model. The key difference in the present work is a modification of the heat balance at the melt/crystal interface to account for radiation through the nearly transparent crystal:

$$(-k_{\text{m}} \nabla T|_{\text{m}} + k_{\text{s}} \nabla T|_{\text{s}}) \cdot \mathbf{n}_{\text{sm}} = \rho_{\text{s}} \Delta H_{\text{f}} \frac{\partial x}{\partial t} (\mathbf{n}_{\text{sm}} \cdot \mathbf{e}_z) + Q, \quad (1)$$

where k_{m} and k_{s} are the thermal conductivity of the BGO melt and crystal, respectively, ρ_{s} is the crystal density, $\mathbf{n}_{\text{sm}}$ is the unit vector normal to the melt/crystal interface, ΔH_{f} is the latent heat of fusion, $\partial x/\partial t$ is the velocity of the melt/crystal interface, and Q represents heat lost by radiation from the interface through the bottom of the crystal.

Due to the lack of a detailed radiation model, Q is treated as a fitting parameter. The walls of the platinum tube below the crucible are at high temperature everywhere due to the high conductivity of this material, so most of the heat is lost by radiation through the hole at the bottom of this tube. Since different locations on the melt/crystal interface have different views of this hole, Q will vary with radial position, with a maximum value at the center axis of the tube. We account for this radial variation using an ad hoc function of the form $Q = A[1 - (R/R_{\text{w}})^N]$, , where R is radial position, and A, N and R_{w} are constants. Once we choose R_{w} and the exponent N, the constant A becomes the only adjustable parameter to be determined by fitting the model to the initial interface position known from experiment. Values of $N = 1, 2, 3$, were tried, as well N equal to infinity (i.e. Q = constant), for $R_{\text{w}} = 50$ mm. Model results were found to be insensitive to the value of N. Simulations reported here for the geometry in Fig. 2a were obtained with $N = 2$, and for the geometry in Fig. 2b were obtained with Q = constant.

The governing equations of model I were solved using the code Cats2D [16] in a manner similar to that described in Ref. [15], except that it was necessary to use a new technique to represent the position of the melt/crystal interface, due to its extremely large distortion caused by radiation heat loss. This technique, which we dub the element edge interface method, identifies whether an element belongs to the crystal or melt based on a

comparison of the average temperature in the element to the interface temperature T_i. Elements are re-assigned to the appropriate material at every iteration until convergence is achieved. The interface is then constructed of the contiguous element edges that lie between the melt and crystal, and interfacial flux conditions are applied there as sharp interface conditions. In general these edges will not precisely equal T_i, with the local error being proportional to the local element size. Using highly refined grids, we have compared the new method to our customary front-tracking method, confirming that convergence is first-order in element size. The low order of convergence requires the use of well-refined grids to obtain accurate solutions, but the method is competitive with common diffuse-interface methods such as enthalpy and phase field, which are also typically first-order convergent.

For model II, heat transfer in the crystal, melt, and crucible wall were simulated for the geometry in Fig. 2b. Here too the effect of the gas bubble under the AHP-heater was taken into account, but convection in the melt was neglected. The equations of radiative–conductive heat transfer [17] with diffusely reflecting boundaries were solved, with the crystal treated as a semi-transparent, gray radiating and absorbing medium. The technique of numerical solution of the energy equation is based on the finite difference method and zonal procedure for description of radiation heat transfer [18]. Faceting of the interface was taken into account, with undercooling given by:

$$\Delta T(r) = \Delta T_0 - \frac{\Delta T_0 r^2}{R_f^2}, \tag{2}$$

where r is the radial position, ΔT_0 is axis facet undercooling, and R_f is the facet radius.

Models III and IV were constructed for the 2D and 3D dynamic simulation of facet formation on the melt/crystal interface, and are used to study the effect of facet formation on heat transfer and on the time-dependence of growth rate $V(t)$. The 2D model III was used to simulate (2 1 1) facet crystal growth in the geometry of Fig. 2b for experiments conducted at a cooling rate of 30 K/h [3]. The 3D model IV was used to simulate (1 1 0) facet crystal growth in the geometry of Fig. 2a with a pulling rate of 5 mm/h [4], assuming the entire process takes place with the interface in the upper part of the system. The functional form of $V = F(\Delta T)$, in the singular orientation, was chosen to be either consistent with 2D nucleation or with screw-dislocation driven growth. Both 2D (model III) and 3D (model IV) calculations were achieved using a new algorithmic approach described in Refs. [20,19], respectively. The method involves the application of an interface motion operator, which accounts for the displacement of the melt/crystal interface based on fundamental kinetic mechanisms (2D nucleation, screw dislocation, vicinal growth and rough growth) resulting in a non-uniform and time-dependent kinetic coefficient (β). Several possible singular orientations are considered, based on experimental observations of crystallographic orientations prone to the exhibition of facets. The effects of crucible walls, radiative heat transport and (in model IV) convective heat transport, were neglected in these calculations. A certain degree of realism was captured by applying results from model I (for Fig. 2a geometry) and model II (for Fig. 2b geometry) as boundary conditions of the first kind. Further details about these models and associated physical and numerical parameters can be found in Ref. [21].

3. Discussion of results

3.1. Effect of crystal absorption on the undercooling measurements

Recently reported work [5] based on 1D calculations of spectral intensity of thermal radiation leaving the crystal and on experimental investigation of the importance of crystal length and sample temperature distribution have shown that, if absorptivity of the crystal at the pyrometer wavelength is more than $\alpha_1 > 0.001\,\mathrm{cm}^{-1}$, the effect of absorption and re-radiation in the crystal must be taken into consideration. The 2D model II was used here to analyze this issue. Results (Fig. 3) show that the brightness temperature (T_b), measured by the pyrometer, depends on the value of the absorption coefficient as well as on the

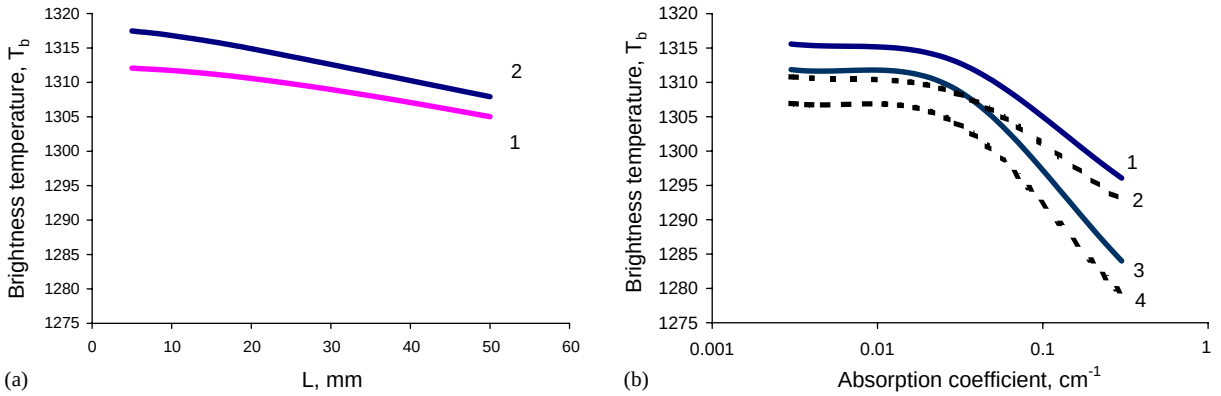

Fig. 3. Changing of brightness temperature with sample length for $\alpha_1 = 0.02\,\mathrm{cm}^{-1}$: (a) 1—2D model [22]; 2—1D model [5]; with absorption coefficient α_1 for sample length equal to 4 cm (b) 1,3—$T_i = 1323$ K; 2,4–$T_i = 1318$K; 1,2—2D model [22]; 3,4—1D model [5].

temperature gradient in the crystal. This effect becomes more pronounced as the crystal length increases. In general, regardless of interfacial undercooling, the pyrometer always underestimates the interfacial temperature value since the crystal always absorbs part of the radiation emitted from the interface and the level of absorption grows with increasing crystalline optical thickness, $\alpha_1 L$, where L is the crystal length. These results have shown that the experimentally measured dynamics of the undercooling ($\Delta T_{\mathrm{exp}}(t)$) strongly depends on the sample's optical thickness, which should therefore be taken into consideration when building the functional dependence $V = F(\Delta T)$.

We have been unable to locate high-temperature data on α_1 of BGO for wavelengths of 0.65, 0.795 and 0.995 μm (operating wavelengths of available optical pyrometers). Such (high-temperature) data was obtained only for the wavelength interval of 1–6 μm [11,12]. In this study the transmittance of BGO single crystalline material, which was used for preparing samples and charge, was measured at room temperature for wavelength intervals of 0.3–0.9 μm and of 2.5–7.0 μm. There are no significant features to report regarding the room-temperature wavelength dependence of α_1 in these two wavelength ranges; it was found that $\alpha_1 = 0.02\,\mathrm{cm}^{-1}$ for all wavelengths examined. Assuming the spectral dependence of α_1 does not change at high temperature for the two ranges of wavelengths examined here, and based on data of work [11] (showing a temperature-insensitive α_1 in wavelength ranges of 1–4 μm), we approximate α_1 to be independent of both temperature and wavelength for all relevant wavelengths. This constant α_1 value ($\alpha_1 = 0.02\,\mathrm{cm}^{-1}$) influences T_b and is therefore applied to the conditions of the experiments reported here in order to correct the experimentally measured ΔT_{exp}.

Fig. 3 shows that the 1D model for the dependence of T_b on sample length agrees well with the 2D model. Therefore we use the 1D model to correct ΔT_{exp} to obtain the undercooling ΔT shown in Figs. 4e and 5f. The value of T_b was estimated using Wien's formula:

$$T_b = \frac{\tilde{n}_2 T_i}{\tilde{n}_2 - T_i \lambda_0 \ln \varepsilon_{\lambda_0}}, \tag{3}$$

where λ_0 is the wavelength of the pyrometer and $\varepsilon_{\lambda_0}$is the spectral "effective" emissitivity of the crystalline sample for wavelengths of the pyrometer. The "effective" emissitivity is determined as the ratio $\varepsilon = I_{\mathrm{rez}}/e_{b\lambda}(T_i)$, where I_{rez} is the spectral intensity of thermal radiation emitted by the non-isothermal sample, and $e_{b\lambda}(T_i)$ is the intensity of blackbody radiation at the interface temperature determined using the Planck formula. The spectral intensity is defined as

$$I_{\mathrm{rez}} = I_{\mathrm{melt}} + I_{\mathrm{cryst}}, \tag{4}$$

where

$$I_{\mathrm{melt}} = \frac{(1 - R_{c-a})(1 - R_{m-c})}{1 - R_{c-a} R_{m-c} e^{-(2\alpha_1)L}} e_{b\lambda}(T_i) e^{-\alpha_1 L}, \tag{5}$$

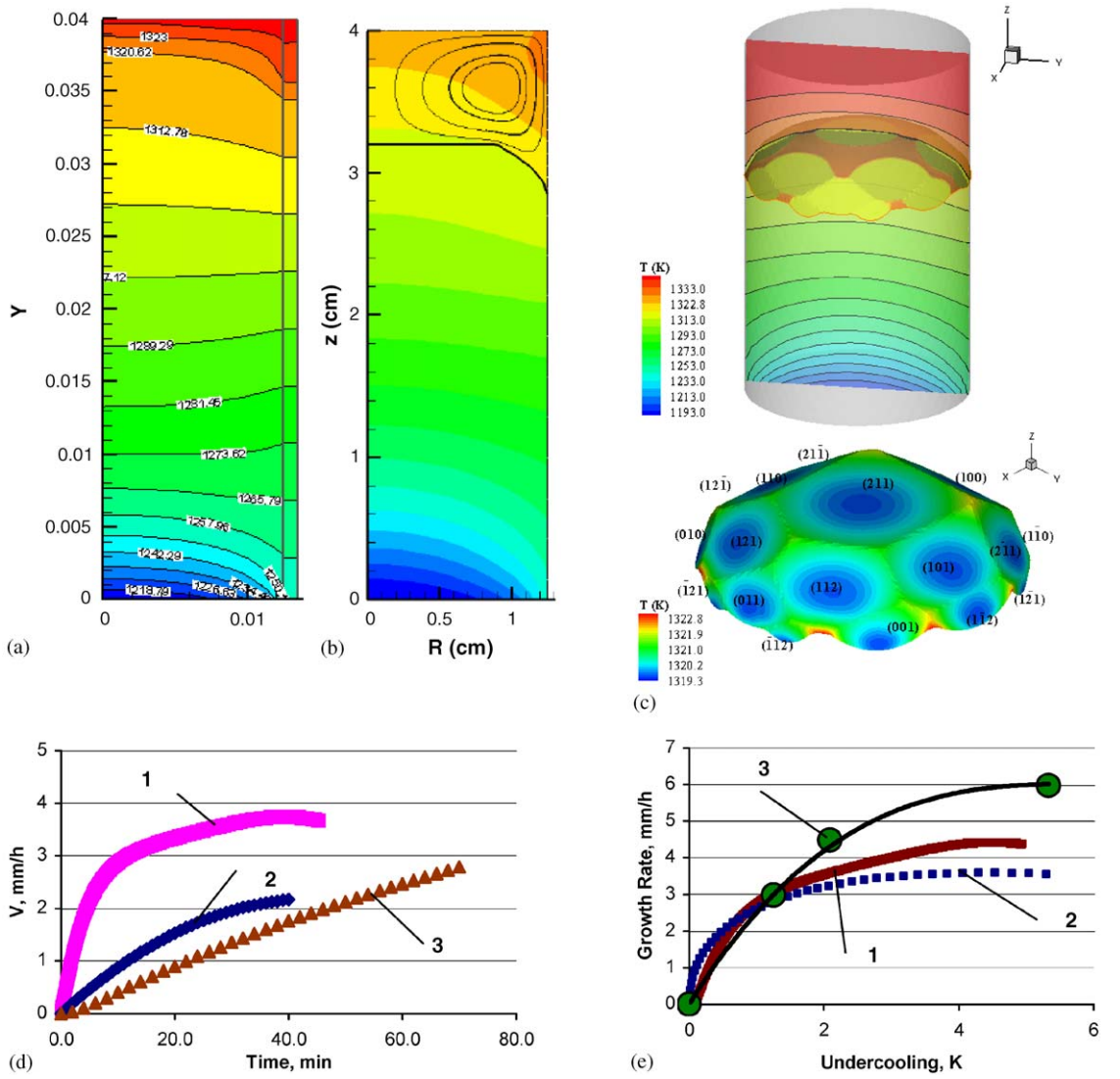

Fig. 4. Temperature field, melt/crystal interface, $V(t)$ and $V(\Delta T)$ dependences during in situ (2 1 1) facet BGO undercooling measurements: temperature field—(a) ii-model, (b) iii-model, (c) iv-model; stream function contours—(b) iii-model, the interfacial morphology—(c) iv-model, $V(t)$ dependence for rate of cooling 30 K/h—(d) i-model (1), ii-model (2), iii-model, dislocation mechanism (3), $V(\Delta T)$ dependence—(e) i-model (1), ii-model (2), 1D model [3] corrected with absorption influence (3).

$$I_{\text{cryst}} = \frac{(1-R_{\text{c-a}})}{1-R_{\text{c-a}}R_{\text{m-c}}\text{e}^{-2\alpha_1 L}} \times \alpha_1 \int_0^L \text{e}_{\text{b}\lambda}\left(T_{\text{i}} - (L-x)\frac{\text{d}T}{\text{d}x}\right) \times \left[\text{e}^{-\int_0^x \alpha_1\,\text{d}x} + R_2\text{e}^{-2\alpha_1 L}\right]\text{d}x, \quad (6)$$

$$\tilde{n}_2 = \frac{h_{\text{P}}c_0}{k_{\text{B}}}, \quad (7)$$

where $R_{\text{c-a}}$ is the reflectivity of the crystal–air interface, $R_{\text{m-c}}$ is the reflectivity of the melt–crystal interface, L is the length of the sample, k_{B} is the Boltzmann constant, h_{P} is the Planck constant,

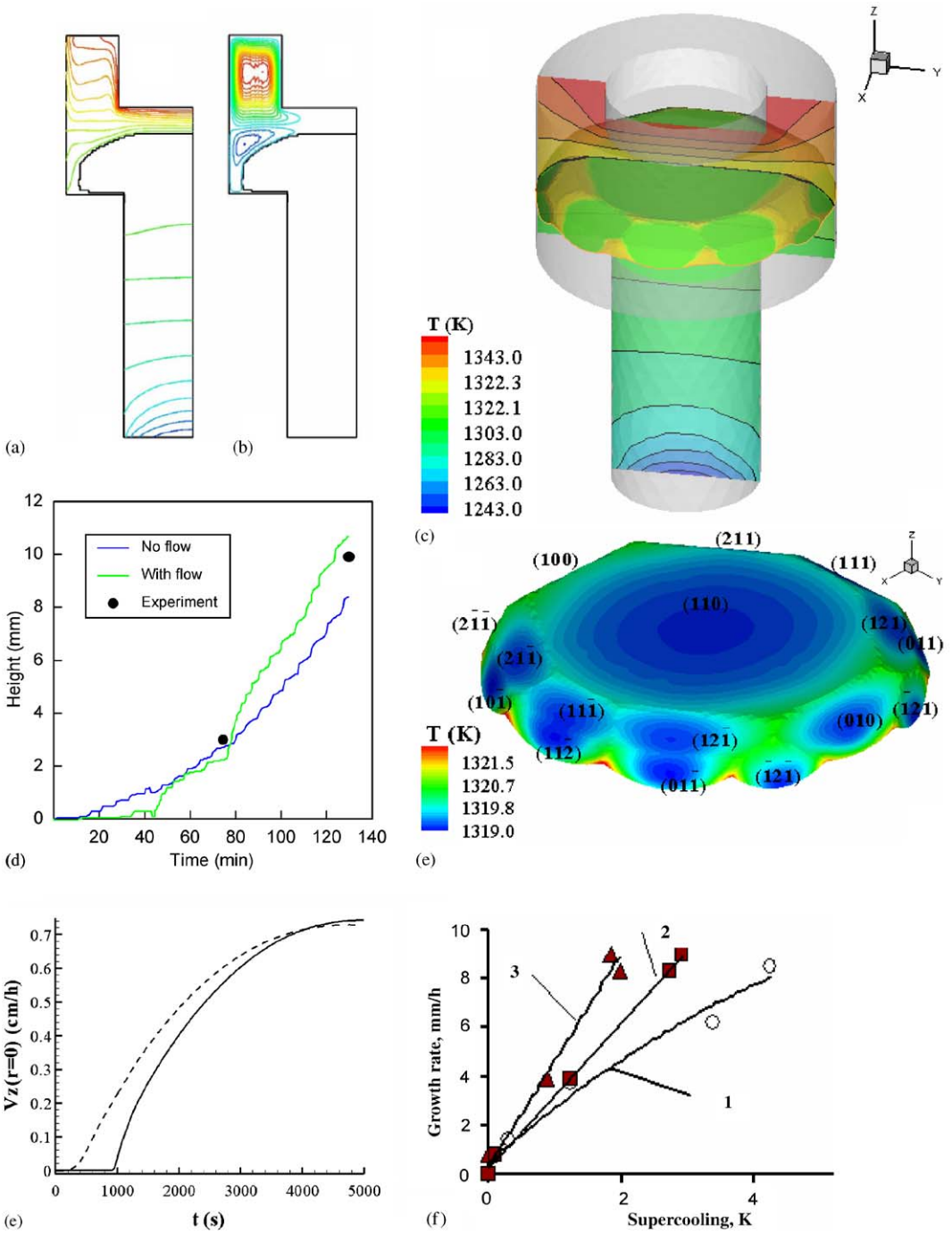

Fig. 5. Temperature field, melt/crystal interface, crystal height $H(t)$, $V(t)$ and $V(\Delta T)$ dependences during in situ (1 1 0) facet BGO undercooling measurements: temperature field—(a) i-model, (c) iv-model; stream function contours—(b) i-model; the distribution of undercooling and interfacial morphology—(c) iv-model; $H(t)$ dependence—(d) i-model; $V(t)$ dependence—(e) iv-model: 2D nucleation, dislocation mechanism; $V(\Delta T)$ dependence—(f) 1D model [4] (1), i-model (2), data i-model corrected with absorption influence (3).

and c_0 is the speed of light in a vacuum, x is the sample axial co-ordinate. This procedure is described in detail in Ref. [5].

3.2. Effect of heat transfer and faceting phenomena on dynamics of growth rate

The results of simulation of heat and mass transfer and of determination of $V(t)$ and $V(\Delta T)$ dependencies for (2 1 1) facet growth for calculation domain shown in Fig. 2b are presented in Fig. 4. The experimental data described in Ref. [3] was used to provide thermal boundary conditions and undercooling data as inputs to these calculations. Figs. 4a–c depict temperature fields and interface shapes predicted by models II, III, and IV, respectively (contours in Figs. 4a and b are plotted on a meridional plane of the axisymmetric domain, with the system centerline at the left edge); results of the different models are generally similar one to another. Calculations of models I (not exhibited here) and III show that the intensity of melt flow in this system is quite small and convection will provide a minimal contribution to the overall heat transfer of the system. This is not surprising when considering the very thin layer of melt and the stabilizing thermal field in which it is immersed. Furthermore, the faceting process does not strongly influence the character of melt flow and, in addition, the influence of the platinum walls is not significant (compare Fig. 4b with Fig. 4a).

Fig. 4d shows BGO crystal growth rate as a function of time for model I (curve 1) and model II (curve 2). For comparison, model III was used to obtain $V(t)$ (curve 3) for the case where there is no faceting on the interface and β is assumed to be isotropic and relatively large in value; curve 3 therefore depicts growth rate for a conduction-dominated system in which kinetics are unimportant. It is notable that the growth rate does not reach a plateau in any of the models, indicating that the melt cooling experiment (method B) is inherently transient in nature. It is also notable that there is a large disagreement between the results of model I and model II. Curiously, the model I simulation exhibits a decrease in growth rate near the end of the simulation (curve 1 in Fig. 4d), a feature not seen in the simulations obtained with the other models. In general, as $\Delta T(t)$ increases, fundamental kinetic mechanisms predict the growth rate to increase with time. However, as $\Delta T(t)$ increases, the interface temperature is lowered, which causes the growth rate to fall behind the rate of motion of the melting point isotherm in the same system. In model I this effect happens to such a large extent that the interface starts melting back, which is an artifact of uncertainty in the model input data for $\Delta T(t)$, as discussed below.

One possible explanation for the disagreement between the models is the formation of a facet in the center of the interface in the model II. Therefore the mean temperature of melt/crystal interface in model II (see Eq. (2)) is less than in model I. The main issue is not faceting per se, but the need to make some kind of assumption about the kinetics as a model input, since neither model can predict these kinetics in a self-consistent manner. Models I and II directly incorporate $\Delta T(t)$ from the experimental measurements, whereas models III and IV base the form of $V(\Delta T)$ on the assumed kinetic mechanism. Data for $\Delta T(t)$ were fitted to a quadratic function for input into model I, but numerical experiments revealed that small changes to the fit caused a large change on the predicted growth rate. This situation is problematic, since determination of the correct form of $V(\Delta T)$ depends on accurate determination of the growth rate, but calculation of the growth rate depends strongly on experimental measurement of ΔT.

Using the data from Fig. 4d, the dependence of BGO growth rate on the undercooling is obtained and plotted in Fig. 4e. In spite of the uncertainty in the growth rate used to obtain $V(\Delta T)$, all of the models predict that growth rate depends sublinearly on interface undercooling, a result which is consistent with previously reported results obtained using a 1D model [2,3,6]. In particular, accounting for radiation heat transfer in the crystal (curve 3 of Fig. 4e) does not change the sublinear character of the dependence for the case of (2 1 1) facet growth; it merely emphasizes it. Thus the results in this work are consistent with arguments made in Ref. [10] regarding possible changes in the interfacial

kinetics mechanism at the growth rate of 5 mm/h for (2 1 1) BGO facet.

The results of simulation of heat transfer and of determination of $V(t)$ and $V(\Delta T)$ dependencies for (1 1 0) facet growth are shown in Fig. 5. The experimental data described in Ref. [4] was used to provide thermal boundary conditions and undercooling data as inputs to these calculations. Model I predictions of temperature field, interface shape, and streamlines are shown in Figs. 5a and b. Model IV predictions of temperature field and interface morphology are shown in Fig. 5c for 2D nucleation (upper image, interface and temperature contours; lower image, interface only). Crystal height vs. time data predicted by model I are shown in Fig. 5d, and model IV predictions of centerline growth rate vs. time, for both 2D nucleation and screw dislocation growth mechanisms, are shown in Fig. 5e. Growth rate computed by various treatments are combined with experimental undercooling measurements to obtain $V(\Delta T)$, as shown in Fig. 5f.

Comparison of Figs. 5a–c shows that interface faceting and melt flow do not have a strong influence on the temperature field in the crystal, yet an interesting phenomenon related to melt convection is observed. At the beginning of growth, a vortex in the gap between the crucible wall and the AHP-heater retards the growth rate, as shown by the crystal height vs. time results plotted in Fig. 5d. Later this vortex is displaced upwards, resulting in a sharp increase in the growth rate. Thus, use of the more exact 2D model accounting for the influence of melt convection on heat transfer results in a significantly different character of $V(t)$ than was obtained earlier [4]. As a result, the dependence $V(\Delta T)$ becomes linear in comparison with slightly sublinear character for 1D and 2D calculations without flow (compare curves 1 and 2 in Fig. 5f). After applying a correction using Eq. (3), which accounts for the variation of brightness temperature with length of the sample, the slope of the linear curve increases (compare curves 2 and 3 in Fig. 5f). These new results suggest a simple kinetic relation exhibiting a constant kinetic coefficient over the range of growth rate values studied using method A. Using these results, we calculate a new estimate of the value of the kinetic coefficient β^{T} for growth of the (1 1 0) facet, equal to 1.0×10^{-6} m/s K in comparison to the value 8.3×10^{-7} m/s K that was estimated earlier [4].

The dynamics of $V(t)$ for facet crystal growth are strongly related to the dynamics of faceting. Fig. 5e shows model IV results for $V(t)$ obtained using the two different kinetic mechanisms that were tested. The results show that in both cases there is an initial transient during which a finite degree of undercooling is formed on the central facet without growth occurring there. As shown in Fig. 5e, the duration of this stage depends on interface kinetic mechanism. Subsequent to this stage of the process, the growth rate on the melt/crystal interface is non-uniform where the facets (and in particular the large center facet) grow at a rate slower than that exhibited by rough portions of the interface. Only during steady-state growth is the (axial) growth rate uniform along the entire interface where a distribution of undercooling is imposed (qualitatively similar to that shown in Fig. 5c), corresponding to a distribution of kinetic coefficient values. Together, these ensure a uniform value of the axial growth rate along the entire interface (see Refs. [19–21]).

The results shown in Fig. 5, as well as additional calculations (not shown here), suggest that the time for establishing steady-state interfacial morphology for BGO is comparable to the time of experiments on undercooling measurements. In this case, the growth rate dynamics associated with faceting, which depend on specific experimental conditions as well as on the type of dominant kinetic mechanism, should be taken into consideration when determining $V(\Delta T)$. Note however that this type of problem requires self-consistent analysis (e.g. by employing an iterative scheme), since modeling of facet formation, needed for the accurate determination of $V(\Delta T)$, requires a priori knowledge of $V(\Delta T)$.

4. Conclusions

Our investigations show that the use of a more exact 2D model predicts a linear $V(\Delta T)$ dependence for the (1 1 0) facet in comparison to

previous work [4], which predicted a sublinear dependence. At the same time, the more exact 2D models for (2 1 1) facet in situ data analysis predict a sublinear $V(\Delta T)$ dependence, which is consistent with previous results. More generally, our investigations of BGO crystal growth demonstrate that accurate determination of growth rate dependence on in situ optical measurements of undercooling, requires an associated thermal model which accounts for combined radiative, conductive and convective heat transport as well as melt/crystal faceting dynamics. Special attention should be given (a) to the effect of optical absorption in the growing crystal on dynamics of the pyrometer signal, and (b) to the effect of melt convection on dynamics of growth rate and (c) to self-consistency between the kinetic functional form of $V(\Delta T)$ assumed when modeling faceting, and experimentally determined undercooling data.

Acknowledgements

The research described in this publication was partially financed by RFBR (Project No. 02-02-17128), by CRDF (Project #RE1-2233), and by INTAS (Project No. 2000-263).

References

[1] V.D. Golyshev, M.A. Gonik, V.B. Tsvetovsky, Instrum. Exp. Tech. 5 (1998) 153.
[2] V.D. Golyshev, M.A. Gonik, V.B. Tsvetovsky, et al., Proceedings of the Academy of Sciences Series, Inorganic Materials, Vol. 6, 1999, p. 715.
[3] V.D. Golyshev, M.A. Gonik, V.B. Tsvetovsky, et al., J. Crystal Growth 216 (2000) 428.
[4] V.D. Golyshev, M.A. Gonik, V.B. Tsvetovsky, J. Crystal Growth 237–239 (2002) 735.
[5] S.V. Bykova, V.D. Golyshev, M.A. Gonik, et al., High Temp.-High Pressures 35/36 (2003/2004), in press.
[6] Ya.V. Vasiliev, V.D. Golyshev, M.A. Gonik, et al., J. Tech. Phys. 70 (5) (2000) 109.
[7] V.D. Golyshev, M.A. Gonik, High Temp.-High Pressures 32 (2000) 581.
[8] V.D. Golyshev, M.A. Gonik, V.B. Tsvetovsky, (Peverhnost) X-ray, Synchrotron & Neutron Researches 11 (2002) 104.
[9] A.A. Chernov, in: M. Cardona, G. Gintherodt (Eds.), Modern Crystallography III, Crystal Growth, Vol. 36, Springer Series in Solid State, Springer, Berlin, 1984.
[10] V.D. Golyshev, M.A. Gonik, V.B. Tsvetovsky, Int. J. Mod. Phys. B 16 (2002) 34.
[11] V.D. Golyshev, M.A. Gonik, High Temp.-High Pressures 26 (1994) 595.
[12] V.D. Golyshev, M.A. Gonik, J. Crystal Growth 262 (2004) 202.
[13] V.D. Golyshev, M.A. Gonik, Crystal Properties and Prep. 36–38 (1991) 623.
[14] S.V. Bykova, V.S. Dozhdikov, V.D. Golyshev, et al., Book of Abstracts, Proceedings of the Xth Russian Conference on Thermophysical Properties, Kazan, 30 September–4 October 2002, pp. 54–55.
[15] A. Yeckel, F.P. Doty, J.J. Derby, J. Crystal Growth 203 (1999) 87.
[16] A. Yeckel, R.T. Goodwin, 2003 Cats2D (Crystallization and Transport Simulator), User Manual (available at http://www.msi.umn.edu/~yeckel/cats2d.html).
[17] V.À. Petrov, N.V. Marchenko, Mater. Sci. (Russia) (1985).
[18] B.I. Deshko, A.Ya. Karvatskii, A.V. Lenkin, Naukovi visti NTUU "KPI" 3 (29) (2003) 20 (in Ukrainian).
[19] O. Weinstein, S. Brandon, J. Crystal Growth, in preparation.
[20] O. Weinstein, S. Brandon, J. Crystal Growth, submitted for publication.
[21] O. Weinstein, Ph.D. Thesis, Technion—Israel Institute of Technology, in preparation.
[22] V.I. Deshko, A.Ya. Karvatskyy, A.V. Lenkin, S.V. Bykova, V.D. Golyshev, M.A. Gonik, V.B. Tsvetovsky, Naukovi visti NTUU "KPI" (in Ukrainian) 4 (30) (2003) 35.